

# UC Berkeley

## UC Berkeley Previously Published Works

### Title

Operando Resonant Soft X-ray Scattering Studies of Chemical Environment and Interparticle Dynamics of Cu Nanocatalysts for CO<sub>2</sub> Electroreduction

### Permalink

<https://escholarship.org/uc/item/0hk569td>

### Journal

Journal of the American Chemical Society, 144(20)

### ISSN

0002-7863

### Authors

Yang, Yao  
Roh, Inwhan  
Louisia, Sheena  
[et al.](#)

### Publication Date

2022-05-25

### DOI

10.1021/jacs.2c03662

Peer reviewed

## Supporting Information

### ***Operando* Resonant Soft X-ray Scattering Studies of Chemical Environment and Interparticle Dynamics of Cu Nanocatalysts for CO<sub>2</sub> Electroreduction**

Yao Yang<sup>1,2</sup>, Inwhan Roh<sup>1</sup>, Sheena Louisia<sup>1,4</sup>, Chubai Chen<sup>1</sup>, Jianbo Jin<sup>1</sup>, Sunmoon Yu<sup>3,4</sup>,

Miquel B. Salmeron,<sup>4,5</sup> Cheng Wang<sup>5,\*</sup>, Peidong Yang<sup>1,3,4,6,\*</sup>

<sup>1</sup>Department of Chemistry, University of California, Berkeley, CA 94720, USA.

<sup>2</sup>Miller Institute for Basic Research in Science, University of California, Berkeley, CA 94720, USA.

<sup>3</sup>Chemical Sciences Division, Lawrence Berkeley National Laboratory, Berkeley, CA 94720, USA.

<sup>4</sup>Department of Materials Science and Engineering, University of California, Berkeley, CA 94720, USA.

<sup>5</sup>Materials Sciences Division, Lawrence Berkeley National Laboratory, Berkeley, CA 94720, USA.

<sup>6</sup>Advanced Light Source, Lawrence Berkeley National Laboratory, Berkeley, CA 94720, USA.

<sup>7</sup>Kavli Energy NanoScience Institute, Berkeley, CA 94720, USA.

\*Corresponding authors: [p\\_yang@berkeley.edu](mailto:p_yang@berkeley.edu), [cwang2@lbl.gov](mailto:cwang2@lbl.gov)

#### **This PDF file includes:**

1. Materials and Methods
2. Figures S1-S15; Table S1
3. References

#### **Experimental section:**

**Synthesis and characterizations of Cu nanocatalysts:** Copper nanoparticles were synthesized using copper(I) acetate (CuAc) and tetradecylphosphonic acid (TDPA) as previously reported.<sup>7</sup> X-ray diffraction (XRD) patterns were acquired on X-ray diffractometer (Bruker D8). Standard XRD patterns of Cu and Cu<sub>2</sub>O can be found from the ICSD database using code numbers #7954 and #63281, respectively. Atomic-scale HAADF-STEM imaging and EELS were performed in a fifth-order aberration-corrected STEM (Cornell Nion UltraSTEM) operated at 100 keV with a beam convergence semi-angle of 30 mrad.

***Operando* soft X-ray-based small angle X-ray scattering (SAXS) measurements.** SAXS measurements were performed in a RSoXS liquid cell setup (Protochips Inc.) with a liquid thickness of around 1 μm previously developed at the Advanced Light Source (ALS) beamline 11.0.1.<sup>29</sup> SAXS data were collected with a back-illuminated Princeton PI-MTE CCD cooled to -45 °C. Scattering patterns of 18 nm NPs were collected for 0.6 s to minimize soft X-ray beam

damage. A 2  $\mu\text{L}$  of 0.1 mg/mL Cu NPs solution was dropcast on the microchip and dried to evaporate residual hexane in a vacuum pump. To demonstrate that *operando* EC-RSoXS cell is suitable to obtain reliable electrochemical measurements, we performed cyclic voltammetry (CV) measurements of Cu NPs supported on a glassy carbon WE in  $\text{CO}_2$ -sat. 0.1 M  $\text{KHCO}_3$ . We used the three-electrode configuration with both the RE and CE made of Pt because of its chemical stability. The distance between the RE and the WE is small to minimize the  $iR$ -drop in a sub- $\mu\text{m}$  electrolyte while the CE has a large surface area to enable rapid polarization. Scattering patterns of the 18 nm NP ensemble were collected for 0.6 s to minimize soft X-ray beam damage.

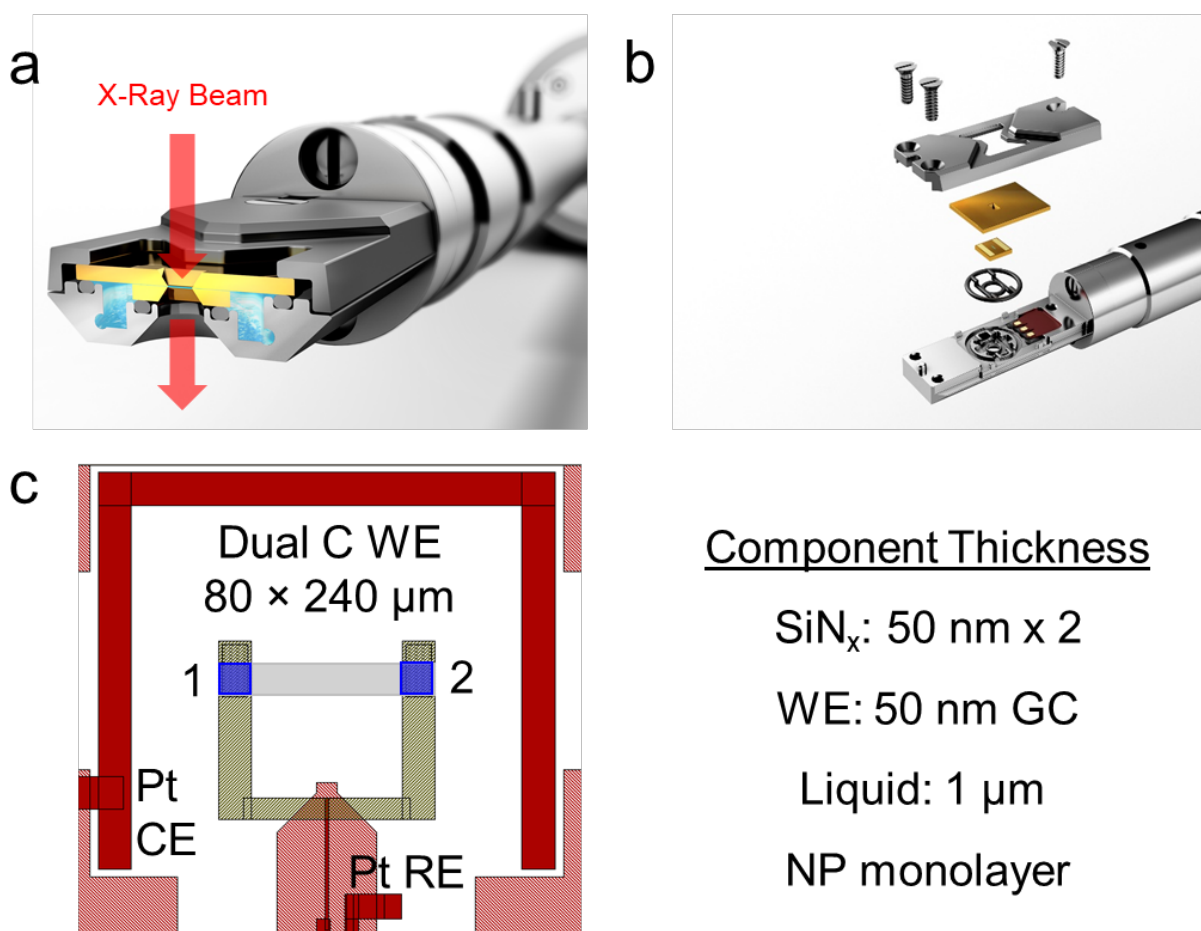


**Figure S1.** (a) Schematic of *operando* EC-RSoXS liquid-cell setup. (b) The layered structure of assembling a typical electrochemical liquid cell (Protochips). (c) The design of the electrochemical liquid-cell microchip with the dual carbon WE, Pt CE and RE. The glassy carbon WE (50 nm) was deposited with monolayer NPs. The shaded rectangular window in blue marks the position of the  $\text{SiN}_x$  window on the same chip. The shaded blue region marks the region of the left glassy carbon (GC) window 1 ( $80 \times 80 \mu\text{m}$ ) facing an X-ray spot of  $100 \times 100 \mu\text{m}$  while the NPs deposited on the

right window 2 serves as a control group, which experience the same electrochemical conditions but without X-ray exposure.

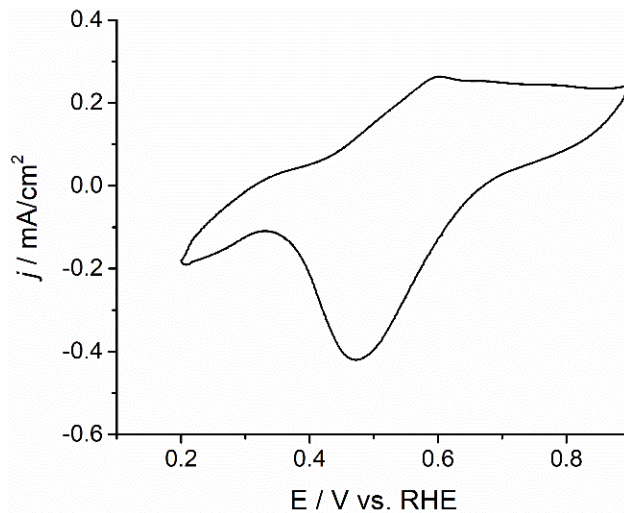


**Figure S2.** CV profile of a 7 nm Cu@Cu<sub>2</sub>O NP ensemble in CO<sub>2</sub>-sat. 0.1 M KHCO<sub>3</sub> at 10 mV/s in a standard electrochemical H-cell. The reduction peak at -0.45 V vs. RHE was assigned to the electroreduction of surface Cu<sub>2</sub>O. The design of the H-cell was used as described previously.<sup>7</sup>

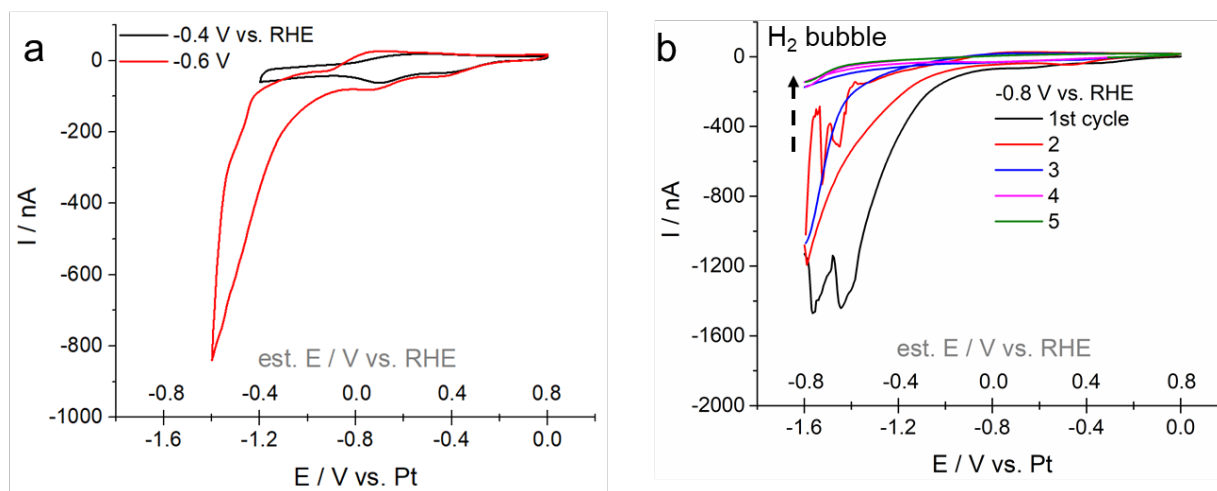


**Figure S3.** CV profiles of the 7 nm NP ensemble in CO<sub>2</sub>-sat. 0.1 M KHCO<sub>3</sub> at 100 mV/s in the EC-RSoXS cell with various lower potential limits of -0.4, -0.6 V vs. RHE in (a) and -0.8 V vs. RHE in (b). After two CV cycles to -0.8 V vs. RHE, a dramatic current decay was observed, indicating the formation of a hydrogen bubble, which is due to the hydrogen evolution reaction (HER) occurring within the CO<sub>2</sub>RR potential range.

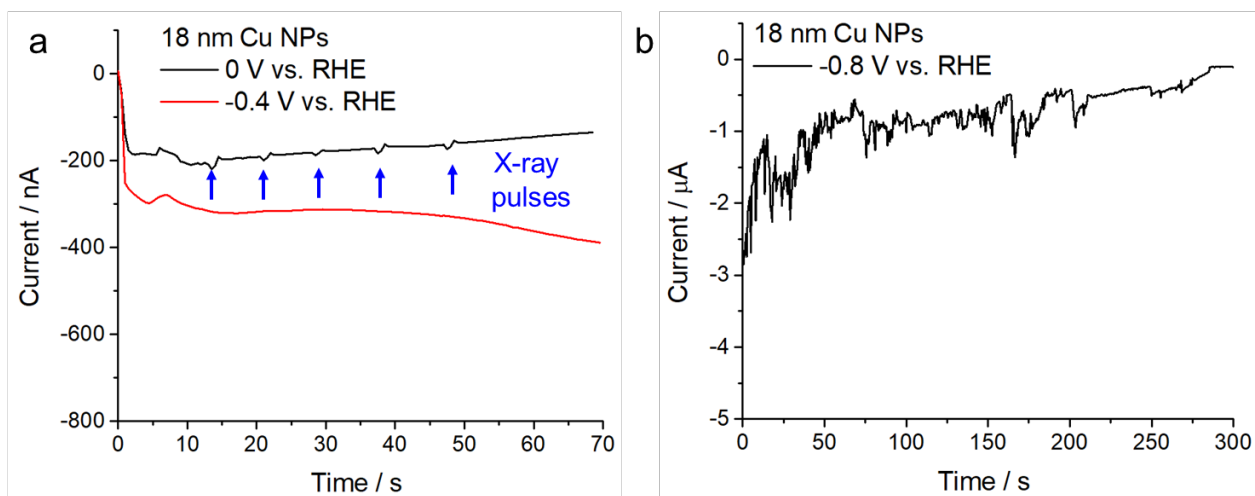


**Figure S4.** CV profiles of the 18 nm NP ensemble with current plateaus at around -200 nA (0 V), -300 nA (-0.4 V), and -1  $\mu\text{A}$  (-0.8 V) in  $\text{CO}_2$ -sat. 0.1 M  $\text{KHCO}_3$ . The spikes, indicated by arrows, are due to photoelectrons generated by X-ray pulses.

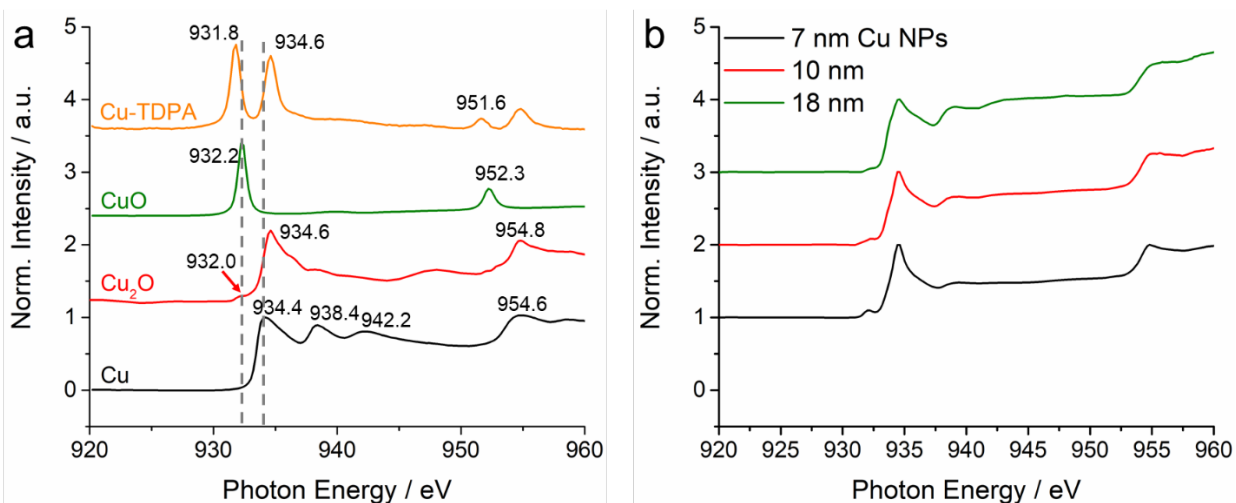


**Figure S5.** (a) XAS spectra of Cu reference samples. (b) Full XAS spectra of Cu  $L_{3,2}$  edges of the 7, 10, and 18 nm NP ensembles.

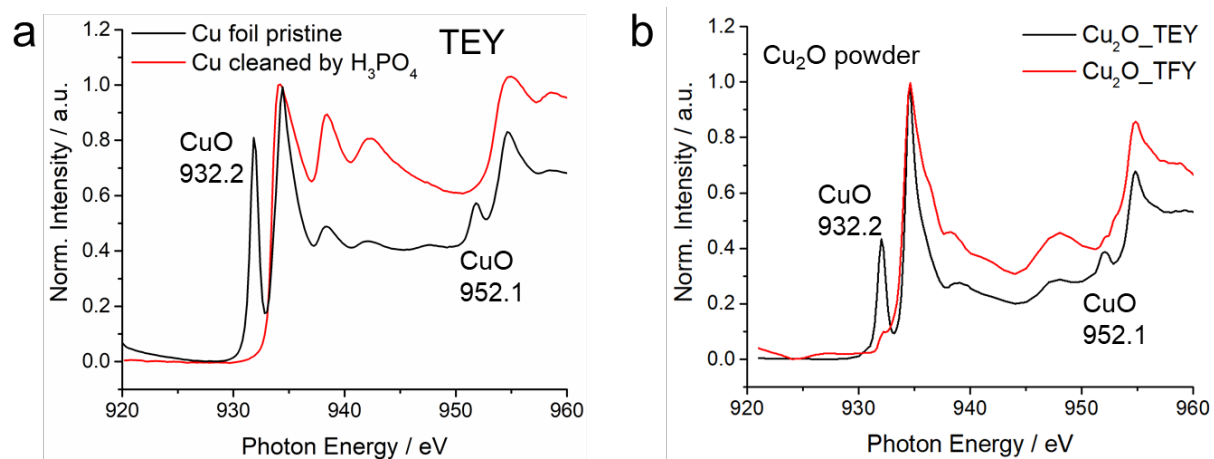


**Figure S6.** (a) XAS spectra of Cu foil in TEY mode. As-received Cu foil has a thin CuO surface layer, so the XAS spectrum was first cleaned by phosphoric acid ( $\text{H}_3\text{PO}_4$ ) and then collected in surface-sensitive TEY mode in order to show the intrinsic metallic surface. (b) XAS spectra of  $\text{Cu}_2\text{O}$  in TEY modes also show the presence of a thin-layer CuO at the surface and that in TFY mode shows the reliable features of bulk  $\text{Cu}_2\text{O}$ .

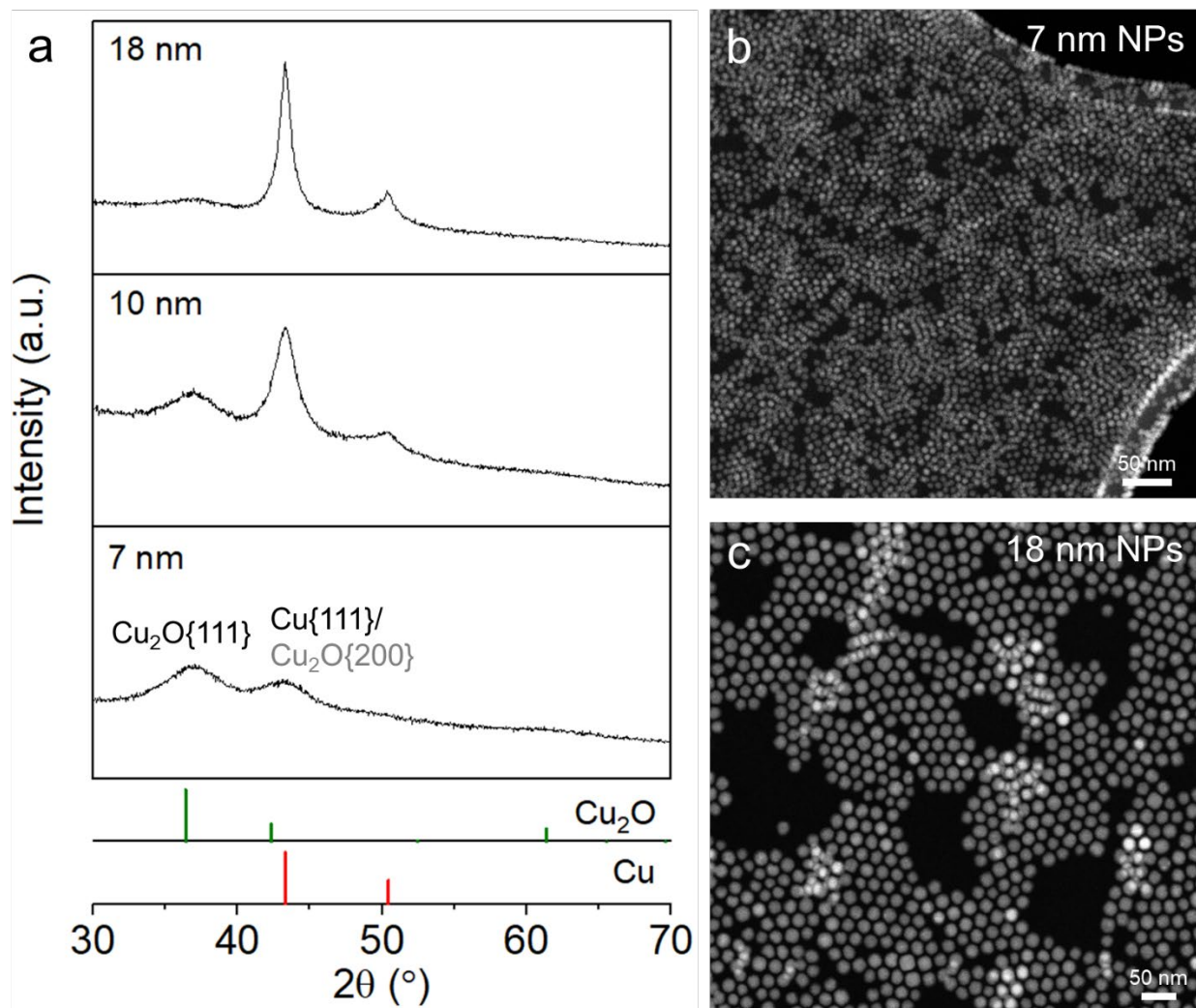


**Figure S7.** (a) XRD patterns of 7, 10, and 18 nm NPs show the increasing fraction of metallic Cu of larger Cu@Cu<sub>2</sub>O NPs. (b-c) Representative low-magnification STEM images of 7 and 18 nm NPs.

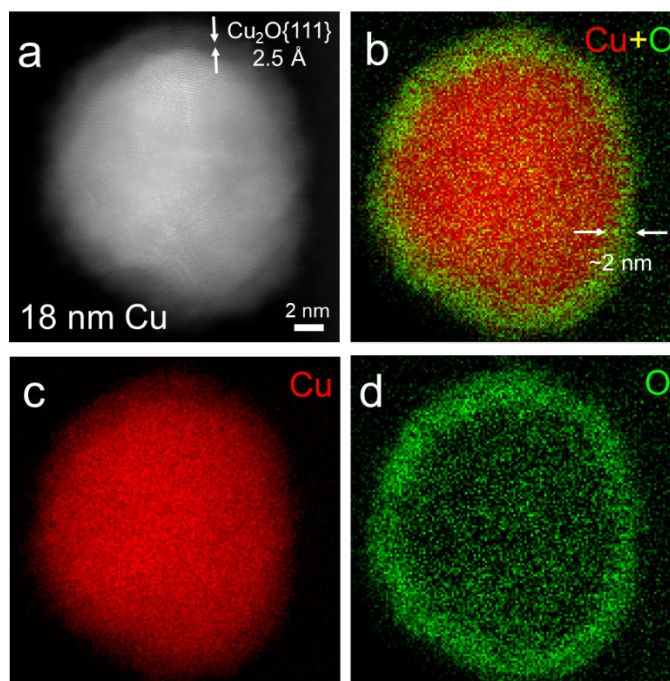


**Figure S8.** STEM images and corresponding EELS elemental mapping of 18 nm NPs with about 2 nm oxide shell.

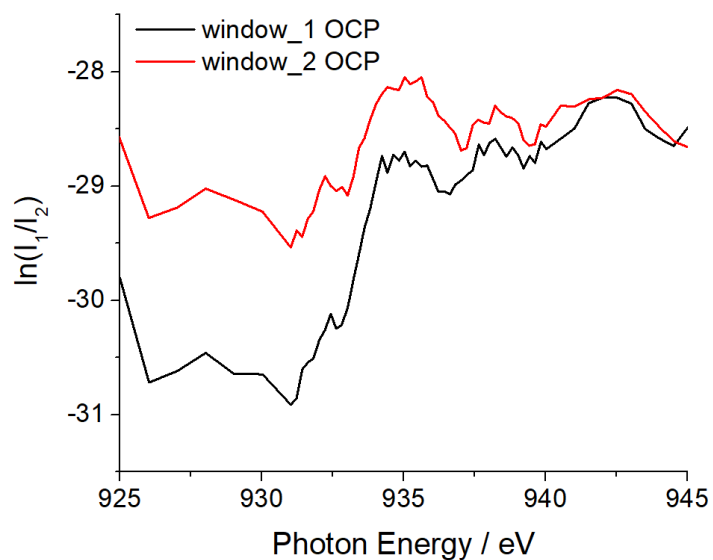


**Figure S9.** Conventional XAS spectra of 7 nm NPs in 1  $\mu\text{m}$  liquid were collected in a transmission mode collected using a photodiode detector. The main edges of  $\text{Cu}_2\text{O}$  at around 934 eV are barely visible in this configuration. The positions of windows 1 and 2 were marked in Fig. S1.

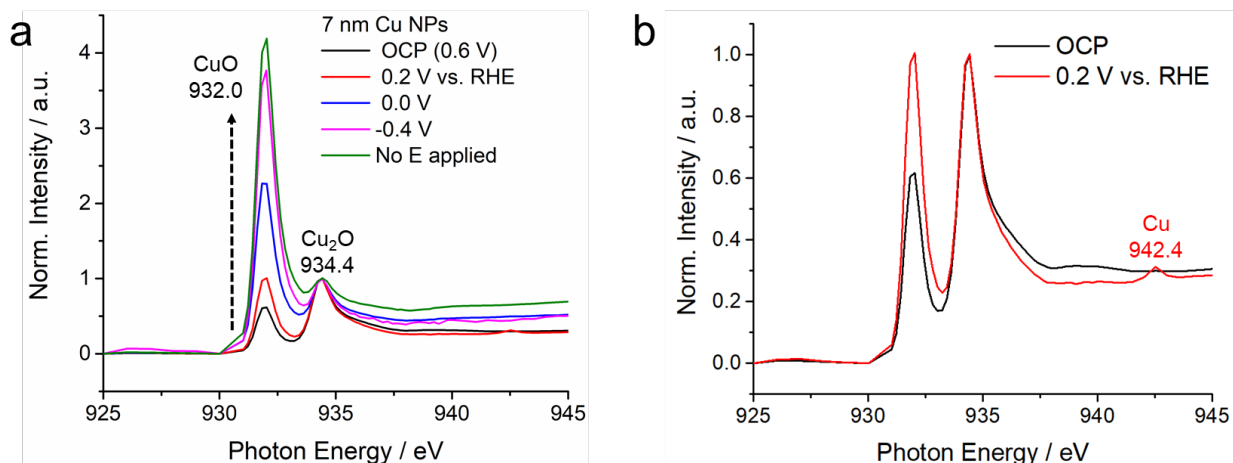


**Figure S10.** (a) *Operando* XAS spectra of the 7 nm Cu@Cu<sub>2</sub>O NP ensemble under various applied potentials from 0.2 to -0.4 V vs. RHE with 12 s per spectrum, showing no electrochemically induced reduction but predominant X-ray induced oxidation to CuO. (b) At 0.2 V vs. RHE, the emergence of a small peak at 942.4 eV indicates that the electroreduction initially converted a minor portion of the NPs into metallic Cu, although the vast majority of NPs were oxidized to CuO by the beam in subsequent XAS acquisition.

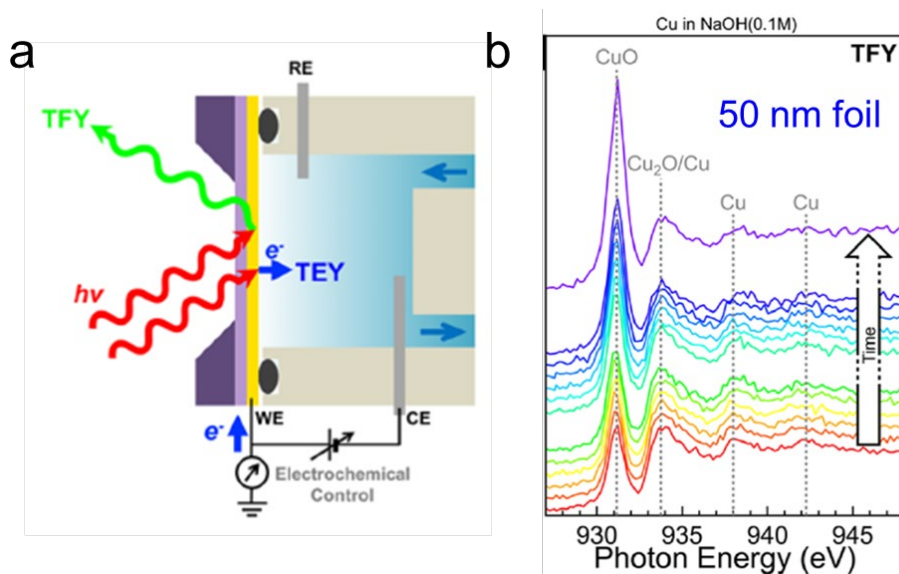


**Figure S11.** Beam-induced oxidation of bulk Cu reported was reported by Salmeron and coworkers.<sup>27</sup> (a) Schematic of a conventional *in situ* XAS electrochemical cell with a bulk Cu film of ~50 nm (yellow) deposited on SiN<sub>x</sub> window (purple). (b) XAS spectra of Cu film in 0.1 M NaOH with ~400 s between the start of each spectrum acquisition, except for ~1300 s between the sixth and seventh spectra and ~2200 s between the penultimate and final spectra. Copyright 2018 American Chemical Society.

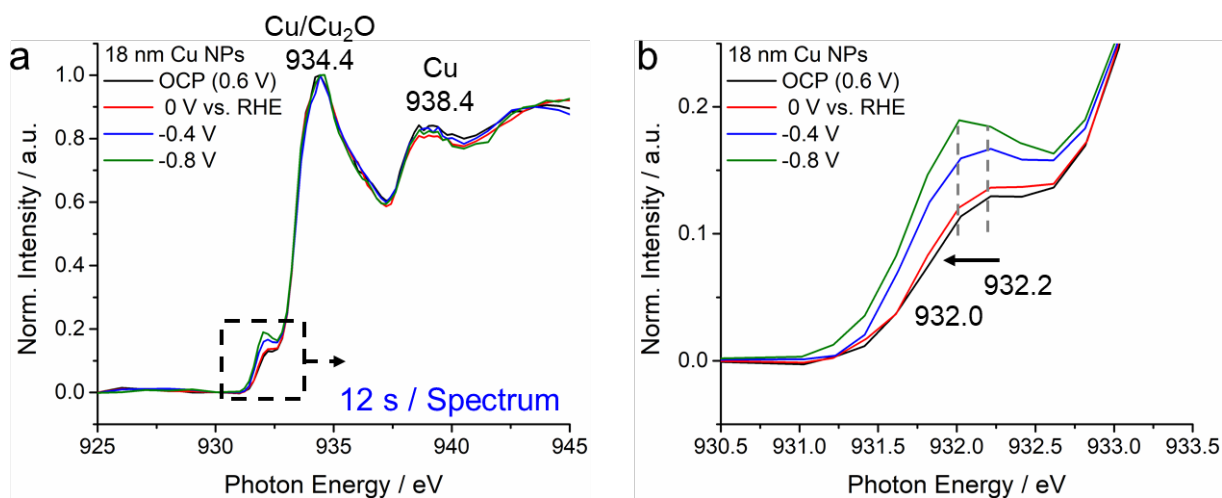


**Figure S12.** (a) *Operando* XAS of the 18 nm NP ensemble with 12 s per spectrum, showing the electroreduction was largely counterbalanced by the X-ray beam induced oxidation. Examinations of pre edges showed a transition from 932.2 to 932.0 eV, indicating a minor formation of metallic Cu (Fig. S6).

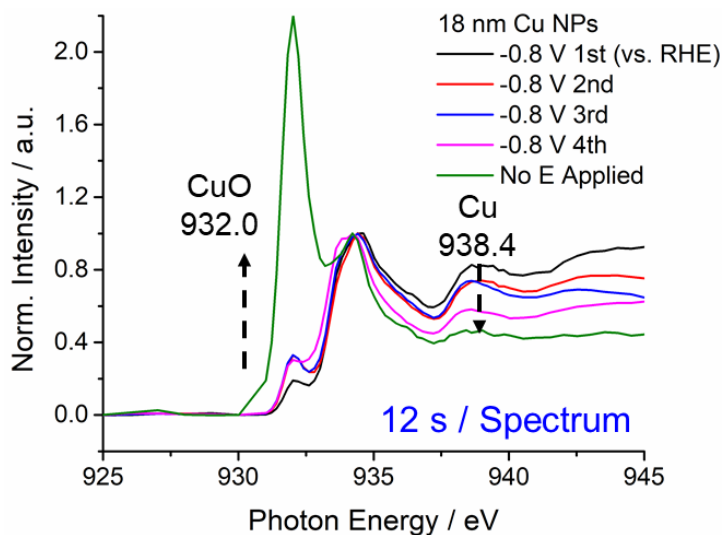


**Figure S13.** *Operando* XAS of the 18 nm NP ensemble with continuous XAS spectra acquisition at -0.8 V vs. RHE, showing the electroreduction was largely counterbalanced by the X-ray beam induced oxidation for the first four XAS spectra. As soon as the potential stopped applying, the X-ray beam-induced oxidation became dominant.

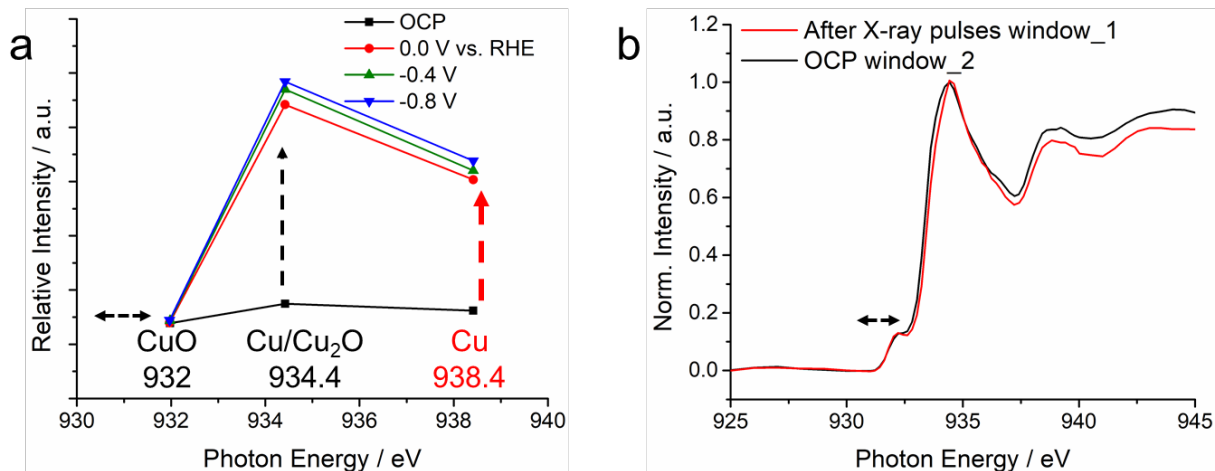


**Figure S14.** (a) *Operando* XAS of the 18 nm NP ensemble (three pulses, 0.2 s each) showing negligible beam-induced oxidation and reliable electroreduction to metallic Cu. (b) Comparison of XAS spectra of NPs at the first window after three sets of X-ray pulses (2.4 s in total) and XAS spectra of Cu NPs without X-ray exposure at the second window, showing negligible X-ray beam-induced oxidation caused by those sub-second X-ray pulses. It should be noted that Cu<sub>2</sub>O also has a minor post-edge peak at 938.4 eV but is significantly lower than that of metallic Cu, thus the intensity change at 938.4 eV can reflect the relative conversion from Cu<sub>2</sub>O to Cu (Fig. 2a).

NP sizes / nm	$q^*$ / nm	$\Delta q$ / nm	$q^* - \Delta q$ / nm
7	10	9.0	1.0
10	15	13.5	1.5
18	22.5	20	2.5

**Table 1.** Measurements of  $q^*$  and  $\Delta q$  values of 7, 10, and 18 nm NP ensembles.